RESEARCH MEMORANDUM

WIND-TUNNEL INVESTIGATION OF STATIC LATERAL AND LONGITUDINAL STABILITY CHARACTERISTICS OF A 1/62-SCALE MODEL OF THE X-1E AIRPLANE AT COMBINED ANGLES OF ATTACK AND SIDESLIP AT SUPERSONIC SPEEDS

By Arthur Henderson, Jr.

Langley Aeronautical Laboratory
Langley Field, Va.

CLASSIFIED DOCUMENT

NATIONAL ADVISORY COMMITTEE
FOR AERONAUTICS

WASHINGTON

September 19, 1957

NACA RM L57G22

NATIONAL ADVISORY COMMITTEE FOR AERONAUTICS

RESEARCH MEMORANDUM

WIND-TUNNEL INVESTIGATION OF STATIC LATERAL AND LONGITUDINAL STABILITY CHARACTERISTICS OF A 1/62-SCALE MODEL OF THE X-1E AIRPLANE AT COMBINED ANGLES OF ATTACK AND SIDESLIP AT SUPERSONIC SPEEDS

By Arthur Henderson, Jr.

SUMMARY

An investigation to determine the static longitudinal and lateral stability characteristics of a 1/62-scale model of the X-1E airplane at combined angles of attack and sideslip has been conducted in the Langley 9-inch supersonic tunnel. Tests were made at Mach numbers of 1.62, 1.94, 2.22, 2.40, and 2.62 on the complete model configuration. Detailed analysis of the test results has not been made in order to expedite publication of the data.

INTRODUCTION

The interference effects of one component of an airplane on another can be very strong and the effects can vary with Mach number and with attitude for any given configuration.

Reference 1 presented the static longitudinal and lateral stability characteristics of a 1/62-scale model of the X-1E airplane at Mach numbers of 1.62, 1.94, 2.22, 2.40, and 2.62. Tests were made through an angle-of-attack range at zero sideslip angle and through an angle-of-sideslip range at zero angle of attack.

The present report investigates the additional effects on the aerodynamic characteristics of the X-1E airplane of combined angles of attack and angles of sideslip. These tests were again performed at Mach numbers of 1.62, 1.94, 2.22, 2.40, and 2.62, and covered the Reynolds number range from 0.36×10^6 to 0.57×10^6 based on the wing mean aerodynamic chord.

SYMBOLS

b	wing span, in.
$\bar{c}$	wing mean aerodynamic chord, in.
C_A	axial-force coefficient, F_A/qS
$C_{D'}$	drag coefficient, $F_{D'}/qS$
C_{D_o}'	minimum drag coefficient
C_L	lift coefficient, F_L/qS
C_l	rolling-moment coefficient, M_X/qSb
C_m	pitching-moment coefficient, $M_Y/qS\bar{c}$
C_N	normal-force coefficient, F_N/qS
C_n	yawing-moment coefficient, M_Z/qSb
C_Y	side-force coefficient, F_Y/qS
D	drag beam of six-component balance
F_A	axial force, lb
$F_{D'}$	drag, lb
F_L	lift, lb
F_N	normal force, lb
F_Y	side force, lb
L_1, L_2	lift beams of six-component balance
M	Mach number
M_X	rolling moment about body axis, ft-lb
M_Y	pitching moment about center of gravity, ft-lb
M_Z	yawing moment about center of gravity, ft-lb
q	dynamic pressure, lb/sq ft

[redacted]

S wing area, sq in.

S_1, S_2, S_3 side-force beams of six-component balance

x longitudinal distance ahead or behind center of gravity, in.

x, y, z Cartesian coordinates fixed with respect to tunnel

X, Y, Z body-axis system

$x/\bar{c}$ longitudinal center-of-pressure location measured from the center of gravity in terms of $\bar{c}$

α angle of attack of body center line, deg

β angle of sideslip, deg

ϵ angle between the body center line and the free stream, measured in the plane of the lift balances, deg

φ roll angle of model, positive clockwise, $\varphi = 0$ when plane of symmetry lies in plane of lift balances, deg

$$C_{l_\alpha} = \left(\frac{\partial C_l}{\partial \alpha}\right)_{\alpha=0}$$

$$C_{m_\alpha} = \left(\frac{\partial C_m}{\partial \alpha}\right)_{\alpha=0}$$

$\frac{\partial C_m}{\partial C_L}$ longitudinal aerodynamic-center location measured from the center of gravity in terms of $\bar{c}$ at $\alpha = 0$, $\frac{\partial C_m}{\partial C_L} = \frac{\left(C_{m_\alpha}\right)_{\alpha=0}}{\left(C_{l_\alpha}\right)_{\alpha=0}}$

$$C_{Y_\beta} = \frac{\partial C_Y}{\partial \beta}$$

$$C_{l_\beta} = \frac{\partial C_l}{\partial \beta}$$

$$C_{n_\beta} = \frac{\partial C_n}{\partial \beta}$$

$\frac{\partial C_n}{\partial C_Y}$ directional aerodynamic-center location measured from the center of gravity in terms of b at $\beta = 0$, $\frac{\partial C_n}{\partial C_Y} = \frac{C_{n_\beta}}{C_{Y_\beta}}$

[redacted]

APPARATUS AND TESTS

Wind Tunnel

The Langley 9-inch supersonic tunnel is a closed throat, single-return, continuous-operating tunnel in which the test section is approximately 9 inches square. Different test Mach numbers are achieved through the use of interchangeable nozzle blocks. Eleven fine-mesh turbulence-damping screens are installed in the settling chamber ahead of the supersonic nozzle. The pressure, temperature, and humidity can be controlled during the tunnel operation.

Model

The model configuration and its geometric characteristics are given in figure 1. The model shown in figure 1 was tested with the horizontal stabilizer at zero incidence only.

The nature of the present tests was such that it was desirable to minimize sting deflections, and consequently the model used during this investigation differed from that of reference 1 in that the aft end of the present model was larger and the rear sections were all circular, in order to accommodate a stronger sting. The model of reference 1 which had a clover-leaf-shaped base, was an exact 1/62-scale model.

Six-Component Balance and Model-Support System

The six-component balance and model-support system used in these tests are described in reference 2.

Tests

Tests were made at Mach numbers of 1.62, 1.94, 2.22, 2.40, and 2.62. The tests were conducted by varying the angle between the body center line and the free stream, ϵ, with the model at various, predetermined roll angles φ. The results were then converted to force and moment coefficients in the body- and stability-axis systems for various combinations of α and β using the relationships presented in the appendix. With the exception of the results at $M = 1.62$, the static longitudinal and lateral characteristics were determined for a sideslip range from about -4° to 12° for constant angles of attack from -12° to 12° in 3-degree increments; and for an angle-of-attack range of about -8° to 12° for constant sideslip angles from 0° to 12° in 3-degree increments. No lateral characteristics are presented at $M = 1.62$ because a mechanical failure occurred in the balance during this phase of the tests.

[redacted]

Precision of Data

The estimated probable errors applicable to the results for the α variable tests at $\beta = 0^\circ$, and to the results for the β variable tests at $\alpha = 0^\circ$ are given in the following table. No attempt was made to estimate the probable errors in the force and moment coefficients at other combinations of α and β because of the complexity of the conversion equations (see appendix).

M	R	C_{F_N}	C_A	C_Y	C_l	C_n	C_m	C_L	$C_{D'}$
1.62	0.41×10^6	±0.0004	±0.0004	±0.0004	±0.0016	±0.0006	±0.0020	±0.0004	±0.0004
1.94	.36	±.0006	±.0005	±.0007	±.0014	±.0010	±.0037	±.0006	±.0005
2.22	.43	±.0005	±.0003	±.0005	±.0010	±.0007	±.0021	±.0005	±.0003
2.40	.49	±.0005	±.0002	±.0004	±.0006	±.0006	±.0013	±.0005	±.0002
2.62	.57	±.0005	±.0002	±.0003	±.0013	±.0008	±.0011	±.0005	±.0002

SUMMARY OF RESULTS

The static longitudinal and lateral force and moment characteristics of the model tested are presented in figures 2 to 6. All the static characteristics are presented in the body-axis system, and in addition C_L, $C_{D'}$, and L/D' are presented in the stability axis system. Each figure consists of two parts: Part (a) presents the variation of the force and moment characteristics with β for various constant angles of attack, and part (b) presents the variation of these characteristics with α for various constant angles of sideslip.

Figure 7 presents the static longitudinal and lateral stability derivatives and the minimum drag coefficients of the model as a function of Mach number. The longitudinal and lateral derivatives of figures 7(a) and 7(b) are taken through $\alpha = 0^\circ$ and $\beta = 0^\circ$, respectively, whereas the lateral derivatives of figure 7(c) are taken through $\beta = 8^\circ$.

Figures 2 to 6 show that the variation of the static longitudinal forces and moments with β is either small or zero at all Mach numbers. Figure 7 indicates that C_{l_α} and C_{D_o}' are relatively unaffected by β, whereas C_{m_α} and $\partial C_m/\partial C_L$ show some variation with β. The large static

[redacted]

margin of the X-1E model throughout the Mach number range and for all sideslip angles tested is also as expected. The largest variations shown in figure 7 are those associated with effects of angle of attack on the lateral derivatives C_{l_β} and C_{n_β}. Although at any given value of M, the variation of C_{l_β} with α is large, the sign always remains negative. Also, the magnitude of the variation decreases with increasing Mach number.

The directional stability data, figures 7(b) and 7(c), have several interesting features. First is the fact that all the curves for $\alpha \leq 0$ show positive directional stability at all Mach numbers; this can be considered similar to the case of an airplane at positive α but with a vertical ventral stabilizer, which is removed from the adverse wing and body interference flow field to which the conventional vertical stabilizer is subjected at positive angles of attack. Second, for angles of attack greater than zero the directional stability of the model was either neutral or unstable for Mach numbers somewhat greater than 1.6. And third, for all positive angles of attack, the neutral or unstable regions encountered exist only within a limited β range. Even for the case where $\alpha = 3^\circ$, which is severely unstable, the instability exists only within the β range of about $\pm 2^\circ$ to 3° (see the C_n curves of figs. 3(a) and 4(a) for $\alpha = 3^\circ$). Figure 7(c) shows that at $\beta = 8^\circ$, the model is directionally stable at all angles of attack.

Langley Aeronautical Laboratory,
National Advisory Committee for Aeronautics,
Langley Field, Va., July 2, 1957.

[redacted]

APPENDIX

CONVERSION OF SIX-COMPONENT EXTERNAL BALANCE MEASUREMENTS TO FORCES ALONG AND MOMENTS ABOUT MODEL BODY OR MODEL STABILITY AXES

The six force balances of the six-component balance described in reference 2 are designated L_1, L_2, D, S_1, S_2, and S_3. Their positions and lines of action are fixed with respect to one another and with respect to the tunnel. A schematic of their reaction force vectors is shown in figure 8 with the origin at some arbitrary moment reference location; that is, it corresponds to the origin of the model body-axis system. The arrows indicate the direction of positive lift, side force, and drag on the balances which would result from the model being at positive ϵ and positive φ in the tunnel. The x-axis coincides with the tunnel center line and it is positive in the positive flow direction. Obviously, the points of application of the loads on the balance do not act as shown in the figure. However, their lines of action pass through the points shown, and since it is immaterial where on a line of action the force is taken to act, they were located as shown for convenience.

The model has two attitude variables: ϵ, the angle between the model body axis and the free stream, in the plane of the L_1 and L_2 balances (tunnel xz-plane), and φ, the angle of roll about the model body axis. The angle φ is positive clockwise when the model is viewed from the rear. The angle φ is zero when the model plane of symmetry lies in the tunnel xz-plane and the model Z-axis coincides with, or makes an acute angle with the tunnel z-axis. The model body axes are defined thus: X-axis coincides with the body center line and is positive rearward; the Y-axis is normal to the X-axis and is positive outboard along the right wing panel; and the Z-axis is mutually perpendicular to X and Y, lies in the plane of symmetry of the model, and is positive upwards. Choosing the direction of the axes in this manner caused the balances to indicate positive numbers when positive forces were involved. The relationship of the body axes to the tunnel axes systems when the model is at positive ϵ and positive φ is illustrated in figure 9.

From the definition of α and β, it can be shown that

$$\sin \alpha = \frac{\cos \varphi \sin \epsilon}{\sqrt{\cos^2 \varphi + \sin^2 \varphi \cos^2 \epsilon}} \qquad \text{(A1)}$$

[redacted]

$$\sin \beta = \sin \epsilon \sin \varphi \tag{A2}$$

Thus the characteristics of a model at combined α and β can be determined by a proper combination of φ and ϵ. The combinations used in this report can be found in figure 10, which was prepared from equations (A1) and (A2). This figure shows only positive values; when α and β are not both positive, the proper sign on φ or ϵ can be determined from equations (A1) and (A2).

The problem of converting the forces measured by the tunnel balances to the forces along and moments about the model body axes was solved with the aid of direction cosines, and are found to be:

$$F_A = D \cos \epsilon - \left(L_1 + L_2\right) \sin \epsilon \tag{A3}$$

$$F_Y = -D \sin \varphi \sin \epsilon + \left(S_1 + S_2 + S_3\right) \cos \varphi - \left(L_1 + L_2\right) \sin \varphi \cos \epsilon \tag{A4}$$

$$F_N = D \cos \varphi \sin \epsilon + \left(S_1 + S_2 + S_3\right) \sin \varphi + \left(L_1 + L_2\right) \cos \varphi \cos \epsilon \tag{A5}$$

$$M_X = \sin \epsilon \left(S_1 x_{S,1} + S_2 x_{S,2} + S_3 x_{S,3}\right) + \cos \epsilon \left(S_1 z_{S,1} + S_2 z_{S,2}\right) \tag{A6}$$

$$M_Z = \cos \varphi \left[\sin \epsilon \left(S_1 z_{S,1} + S_2 z_{S,2}\right) - \cos \epsilon \left(S_1 x_{S,1} + S_2 x_{S,2} + S_3 x_{S,3}\right)\right] + \sin \varphi \left(L_1 x_{L,1} + L_2 x_{L,2}\right) \tag{A7}$$

$$M_Y = \sin \varphi \left[\sin \epsilon \left(S_1 z_{S,1} + S_2 z_{S,2}\right) - \cos \epsilon \left(S_1 x_{S,1} + S_2 x_{S,2} + S_3 x_{S,3}\right)\right] - \cos \varphi \left(L_1 x_{L,1} + L_2 x_{L,2}\right) \tag{A8}$$

The preceding loads and moments are for the body-axis system. The conversion of normal- and axial-force coefficients along the body axis to lift and drag coefficients in the stability-axis system is

$$C_L = C_N \cos \alpha - C_A \sin \alpha$$

$$C_D' = C_A \cos \alpha + C_N \sin \alpha$$

REFERENCES

1. Henderson, Arthur, Jr.: Wind-Tunnel Investigation of the Static Longitudinal and Lateral Stability of a 1/62-Scale Model of the X-1E at Supersonic Speeds. NACA RM L56C23b, 1956.

2. Rainey, Robert W.: Investigation of the Effects of Bomb-Bay Configuration Upon the Aerodynamic Characteristics of a Body With Circular Cross Section at Supersonic Speeds. NACA RM L55E27, 1955.

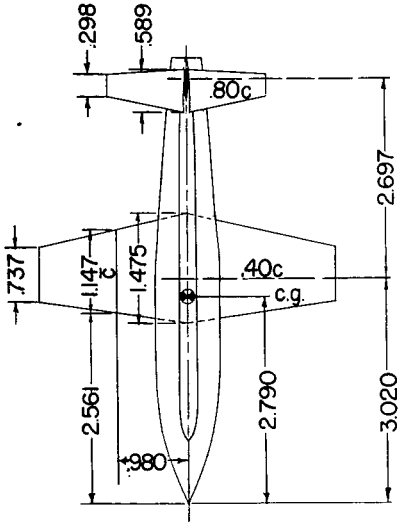

Wing	
Area	4.864 sq. in.
Span	4.410 in.
Aspect ratio	4
Section	modified 64A004
Incidence	2°
Mean aerodynamic chord	1.147 in.
Stabilizer	
Area	.974 sq. in.
Section	65-008
Vertical tail	
Area	.958 sq. in.
Section	65-008

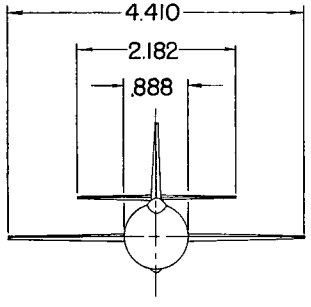

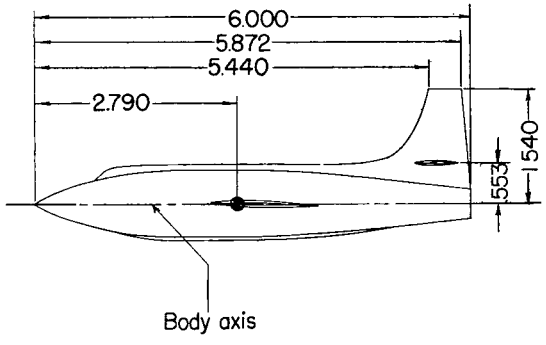

Figure 1.- Three-view drawing of 1/62-scale model of the X-1E airplane. All dimensions are in inches.

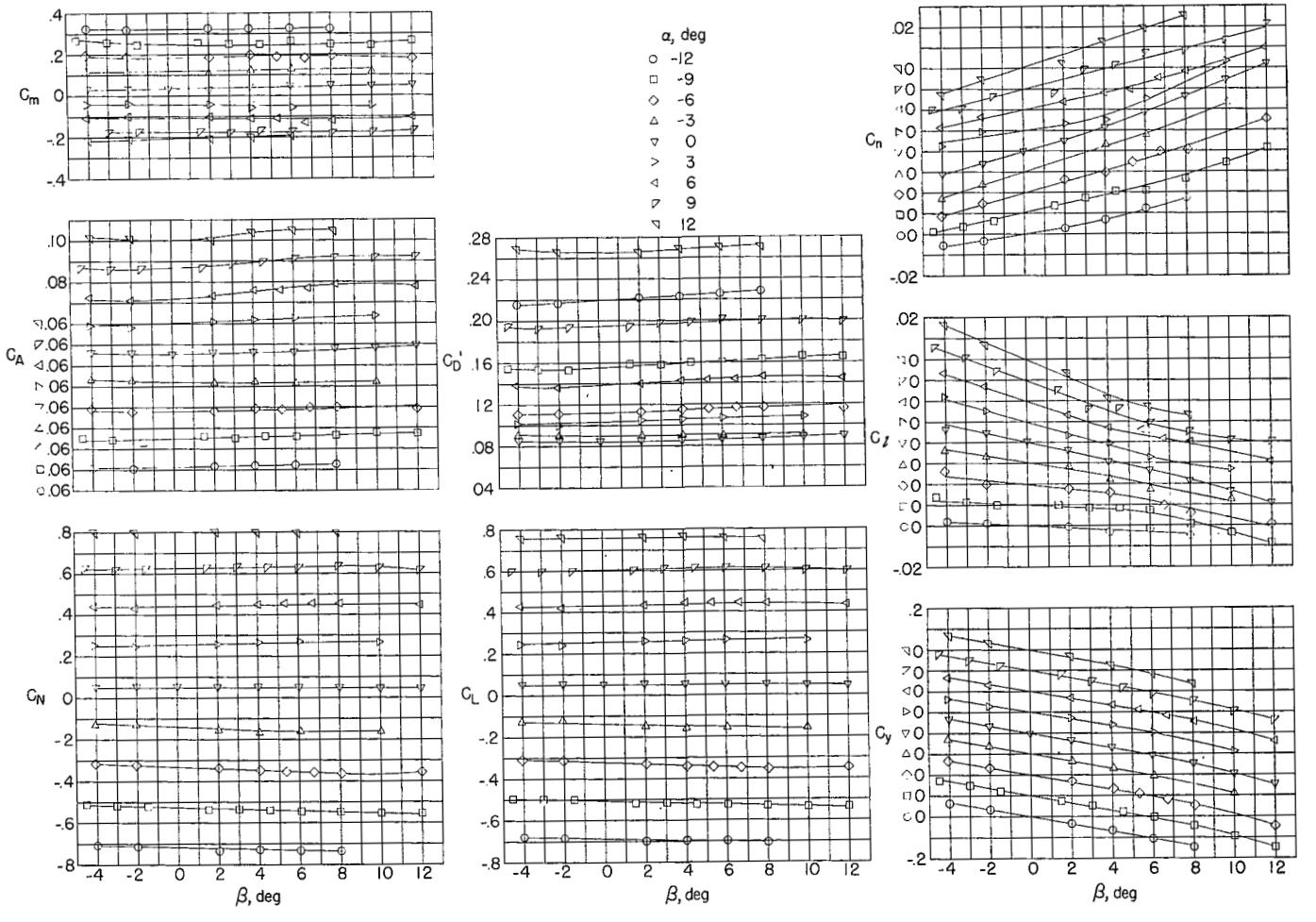

(a) Constant angle of attack.

Figure 2.- Static lateral and longitudinal characteristics of a 1/62-scale model of the X-1E airplane. M = 1.62.

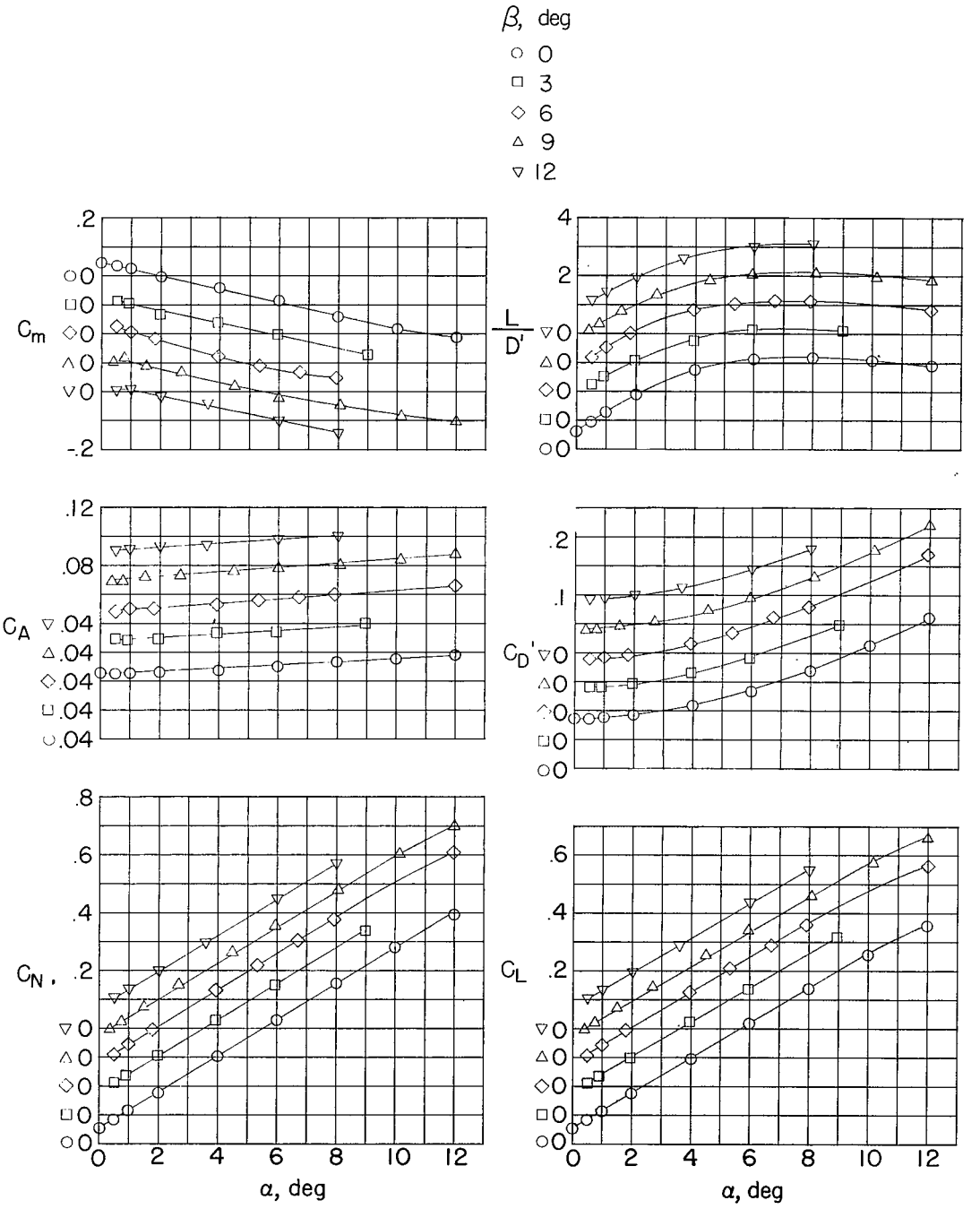

(b) Constant angle of sideslip.

Figure 2.- Concluded.

[redacted]

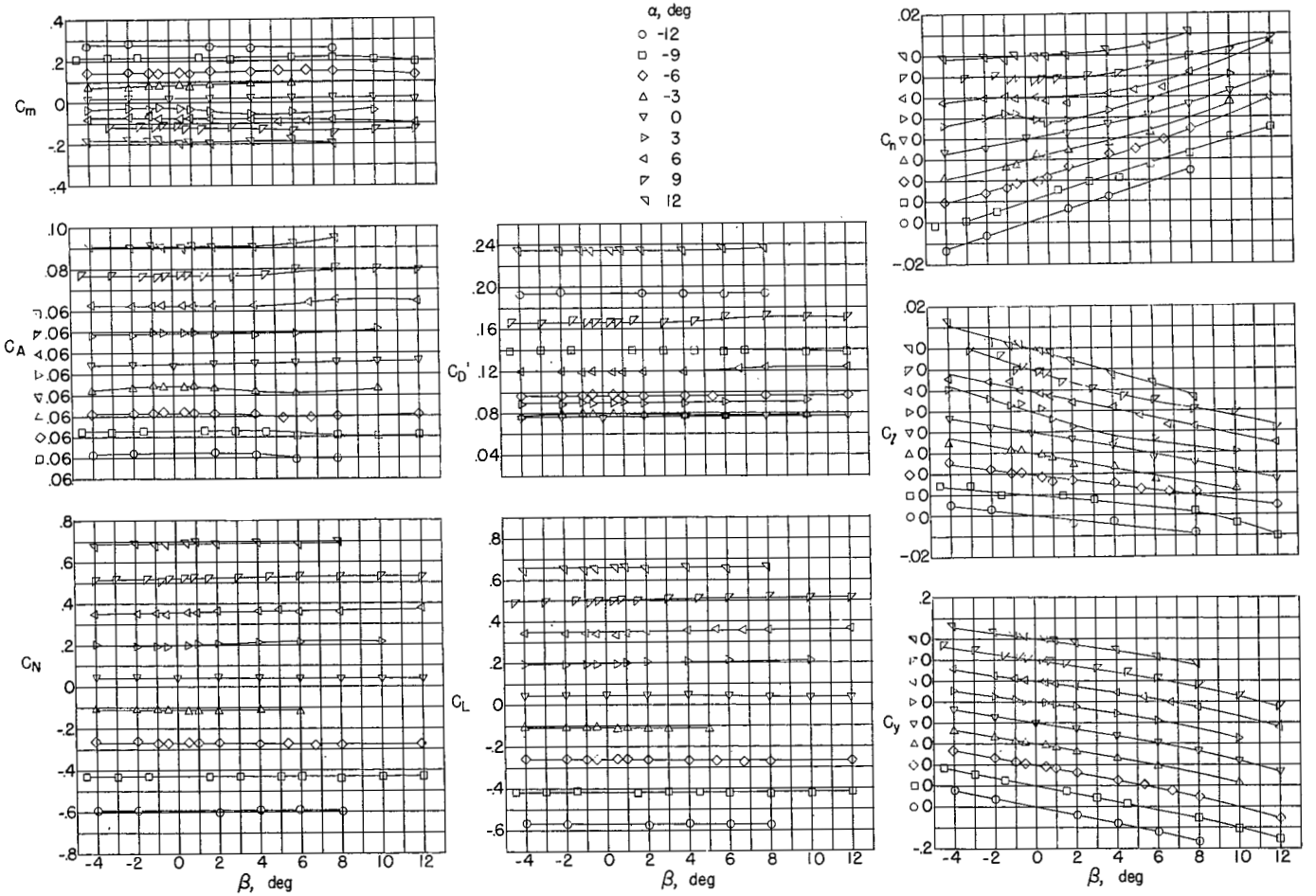

(a) Constant angle of attack.

Figure 3.- Static lateral and longitudinal characteristics of a 1/62-scale model of the X-1E airplane. M = 1.94.

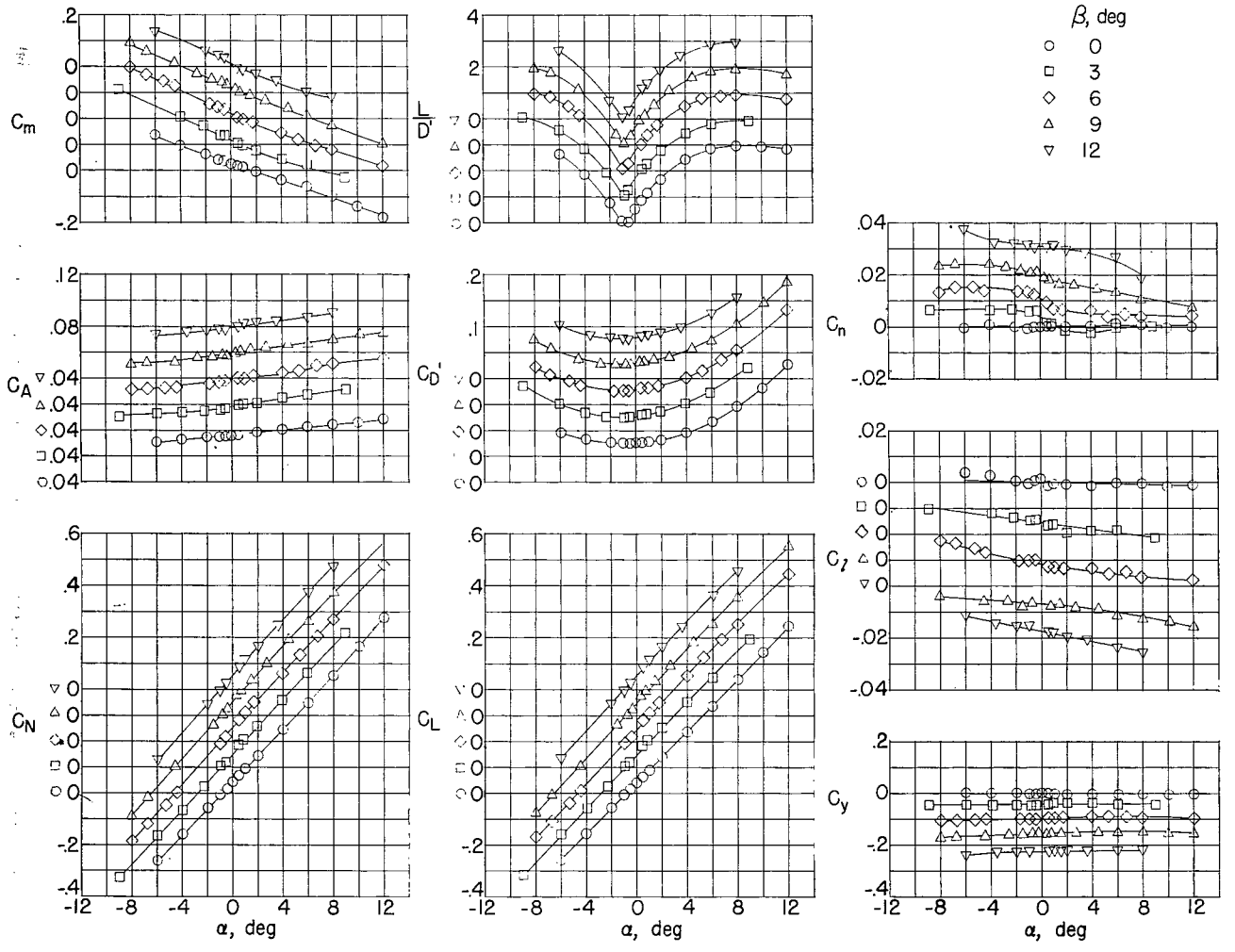

(b) Constant angle of sideslip.

Figure 3.- Concluded.

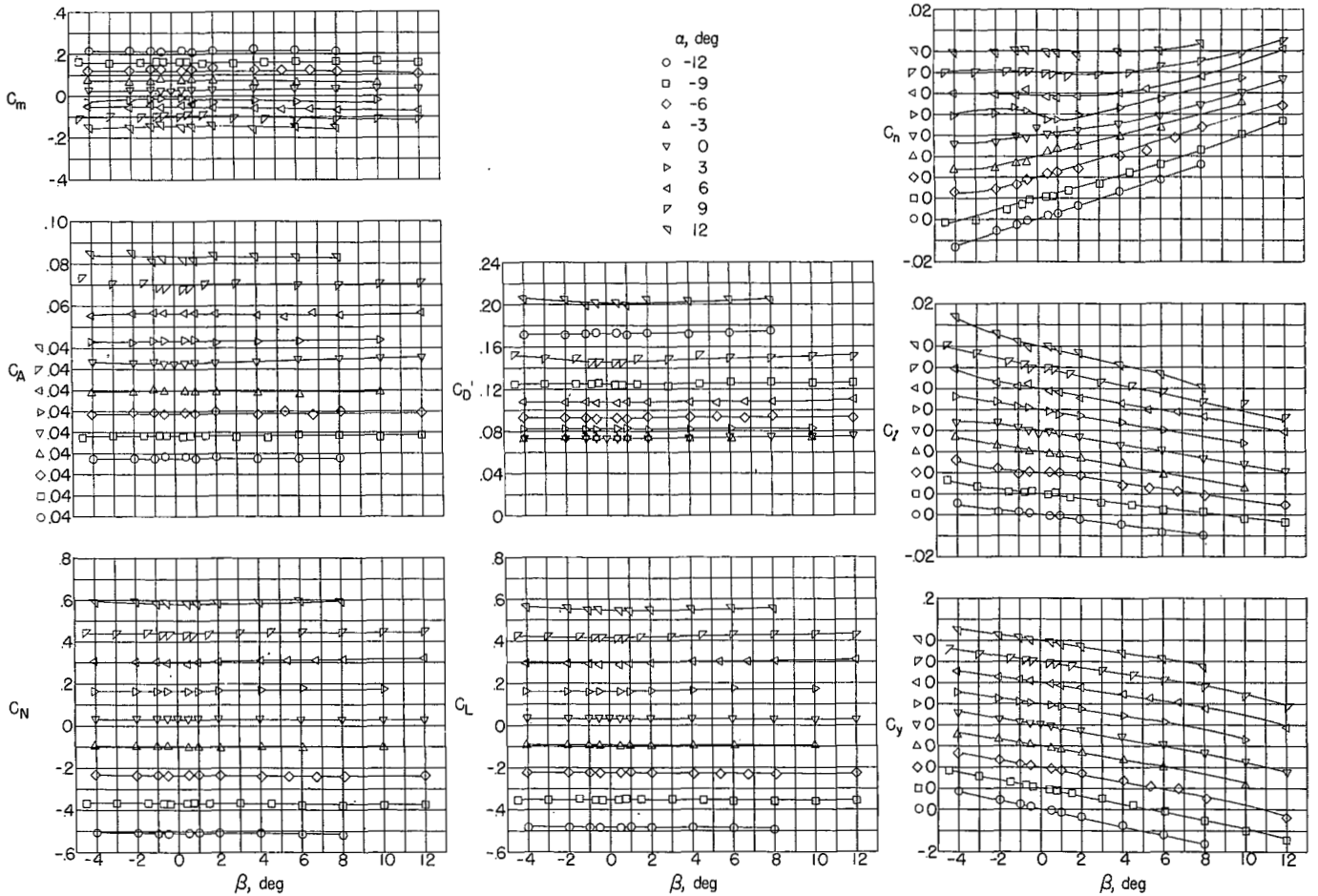

(a) Constant angle of attack.

Figure 4.- Static lateral and longitudinal characteristics of a 1/62-scale model of the X-1E airplane. M = 2.22.

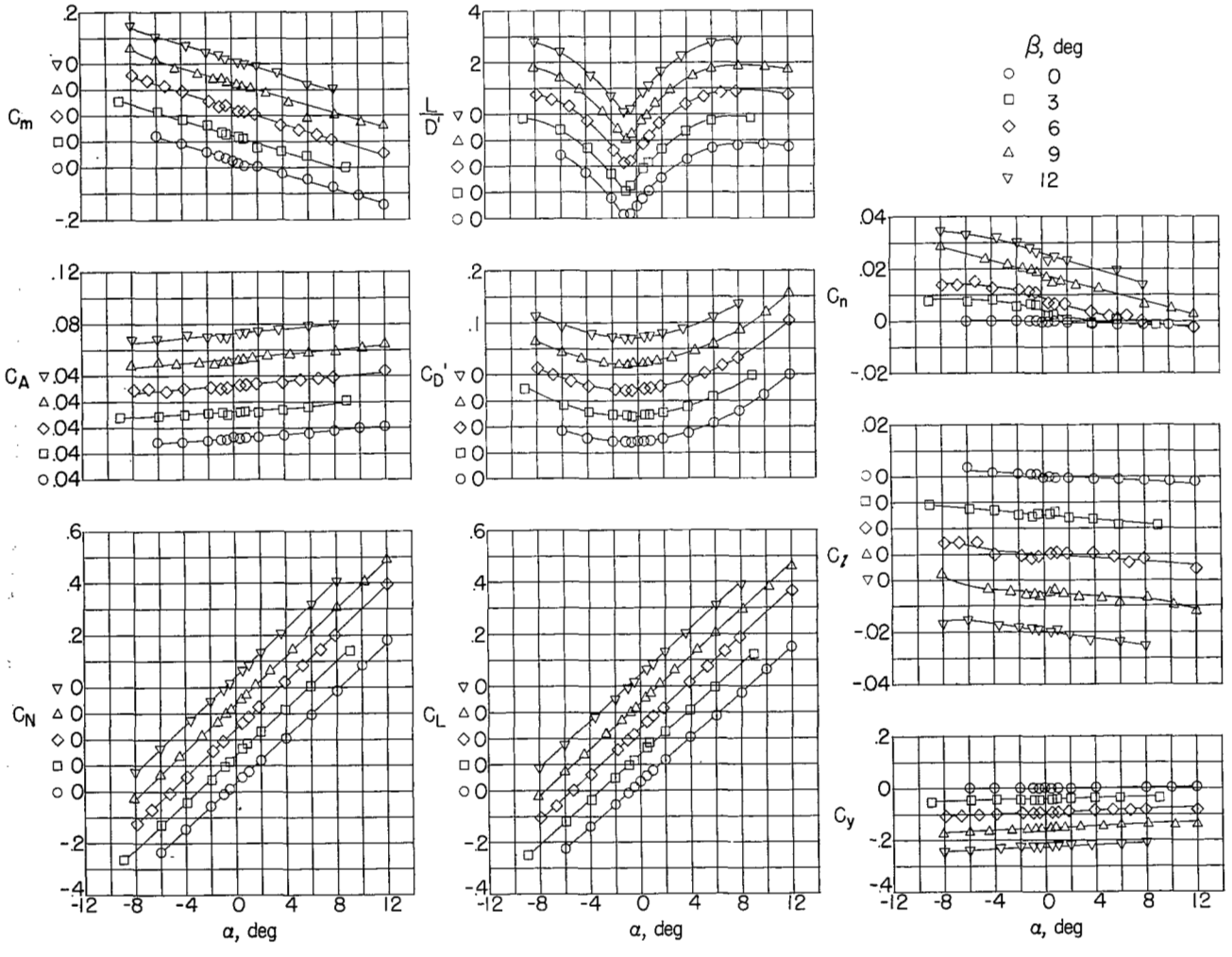

(b) Constant angle of sideslip.

Figure 4.- Concluded.

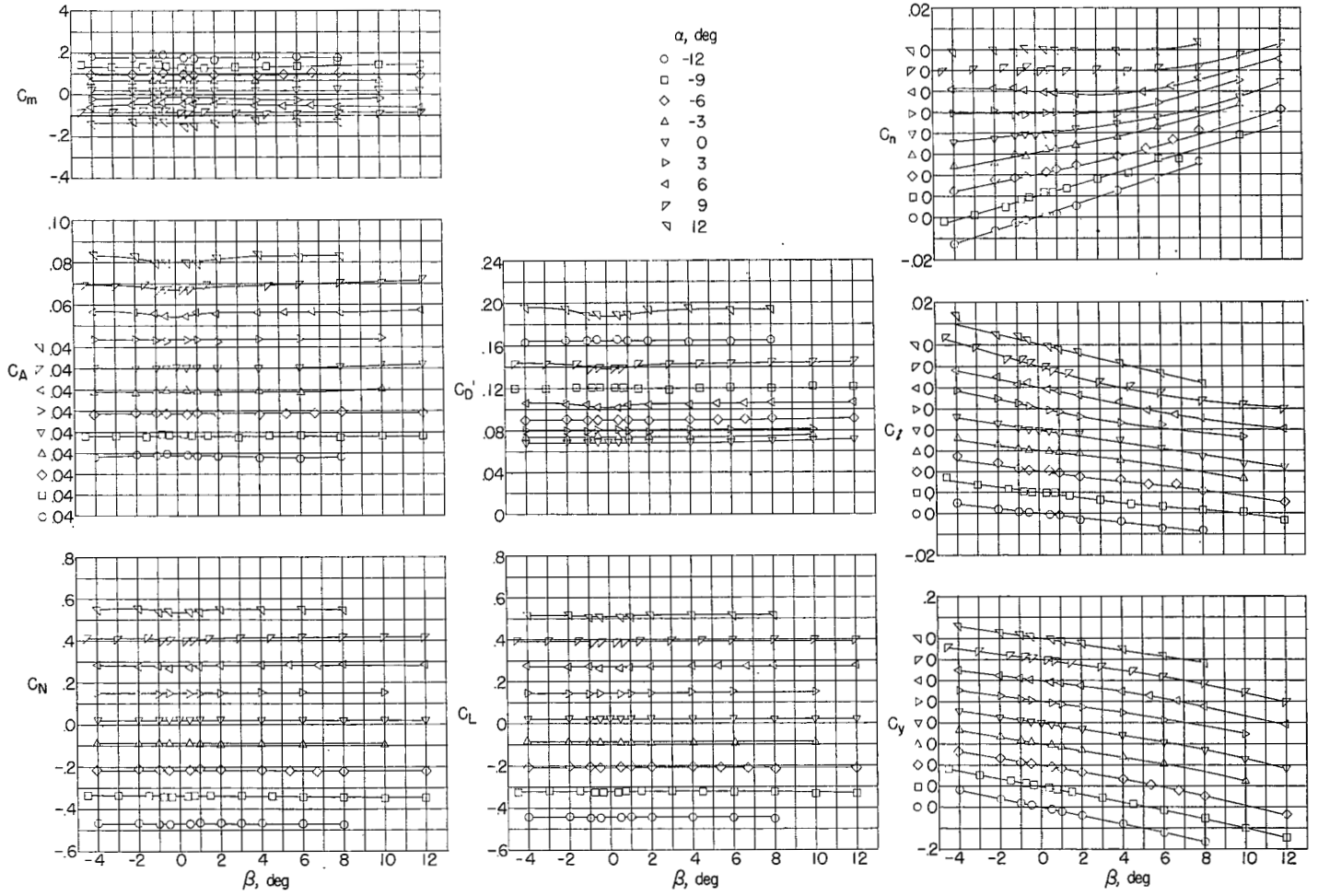

(a) Constant angle of attack.

Figure 5.- Static lateral and longitudinal characteristics of a 1/62-scale model of the X-1E airplane. M = 2.40.

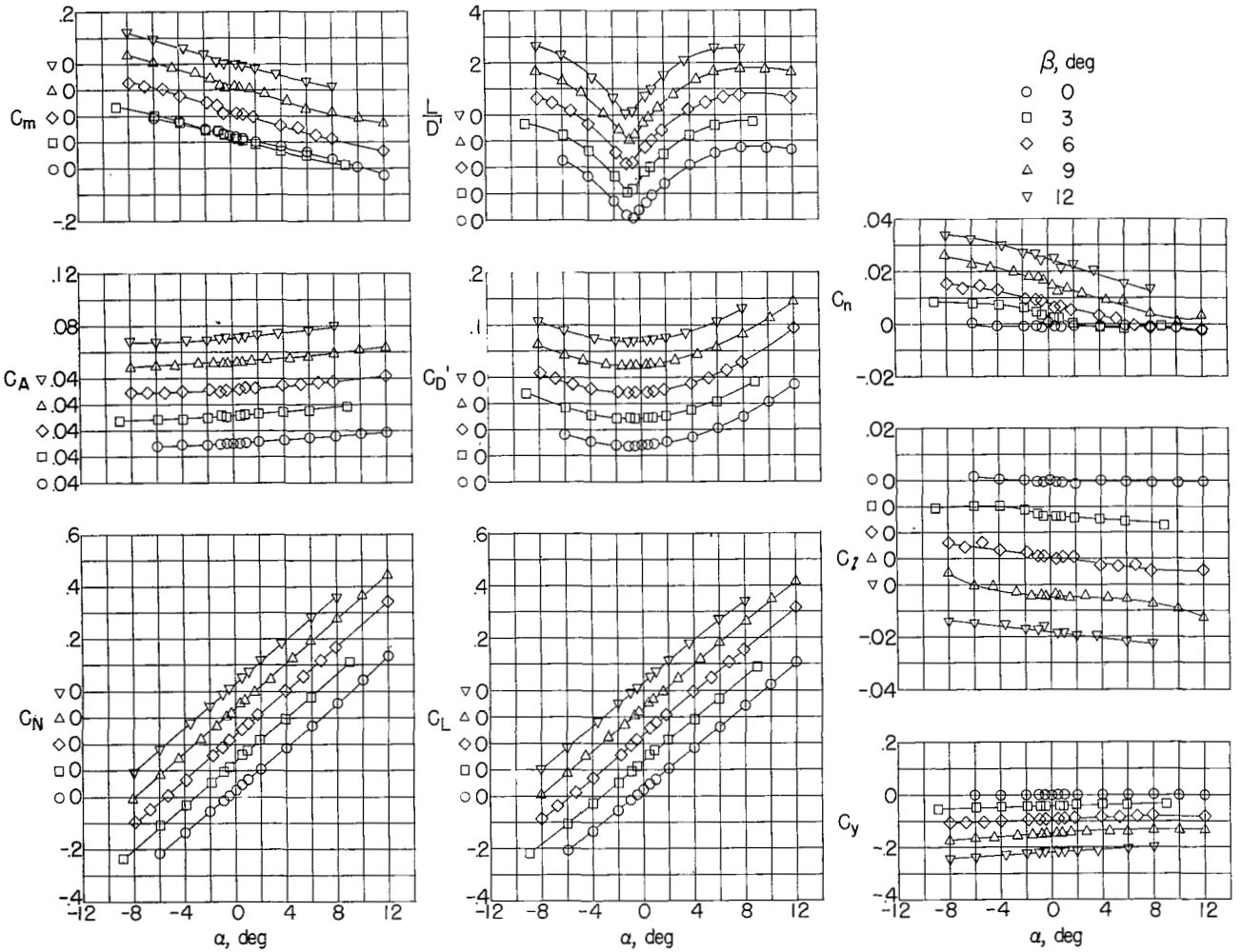

(b) Constant angle of sideslip.

Figure 5.- Concluded.

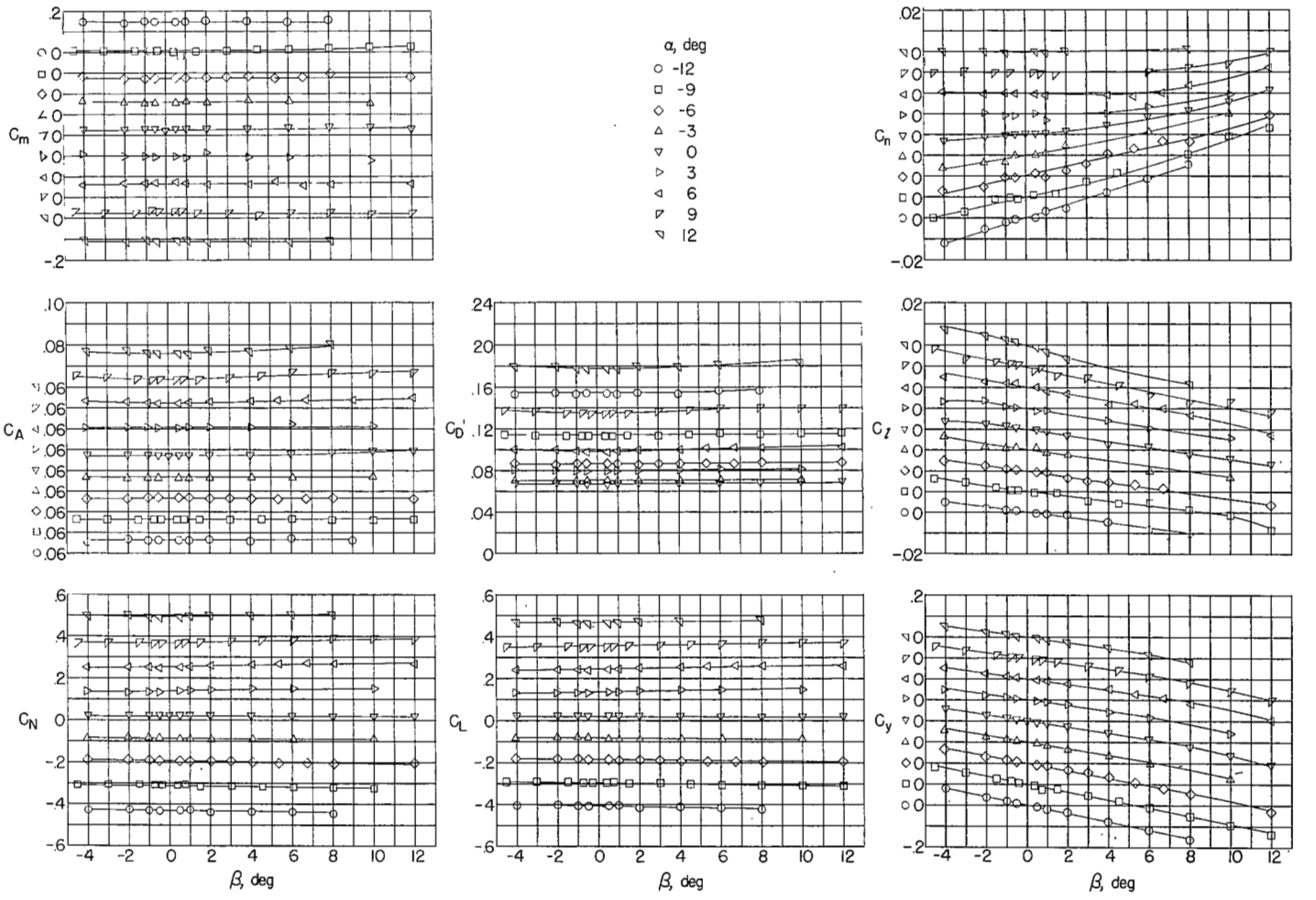

(a) Constant angle of attack.

Figure 6.- Static lateral and longitudinal characteristics of a 1/62-scale model of the X-1E airplane. M = 2.62.

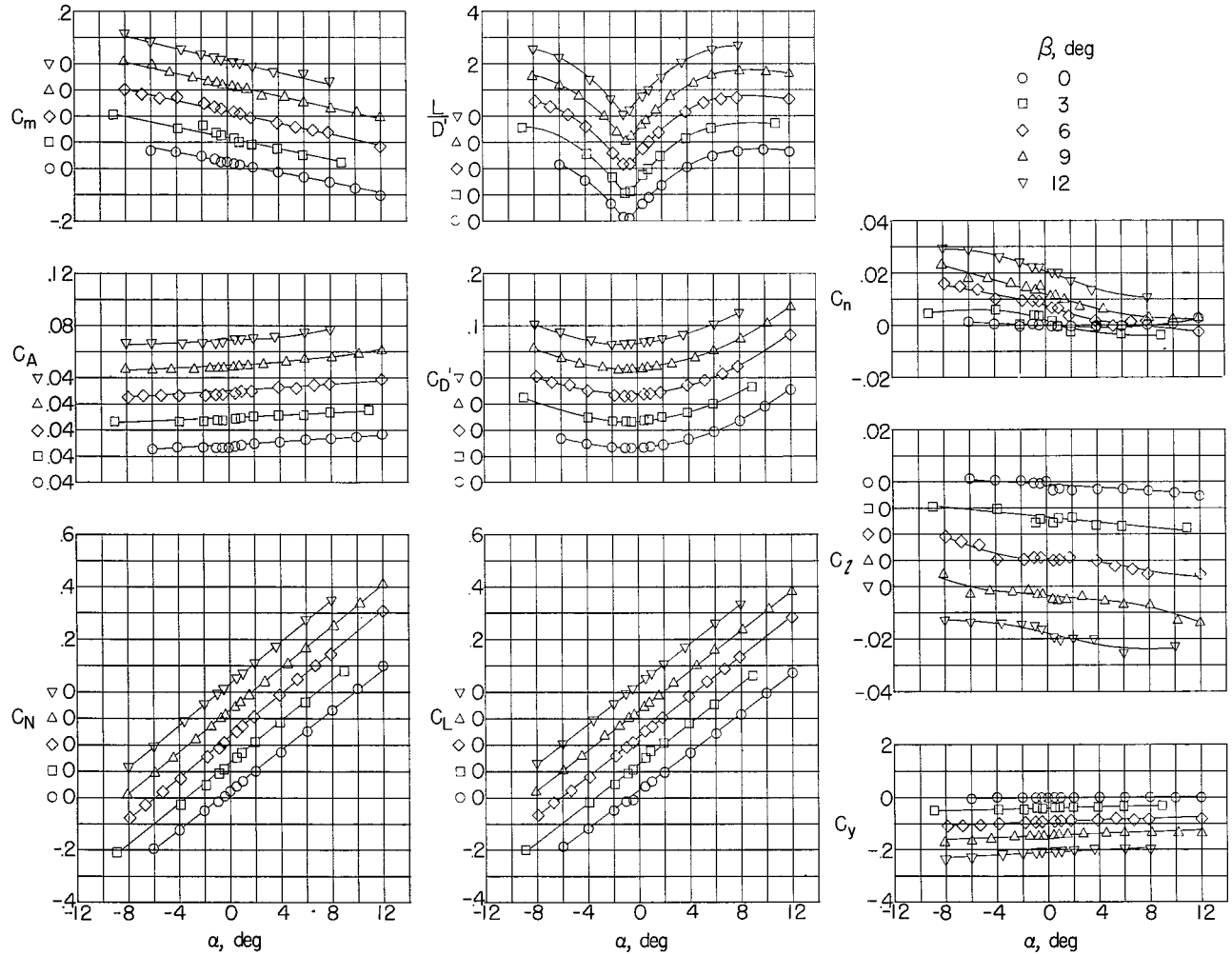

(b) Constant angle of sideslip.

Figure 6.- Concluded.

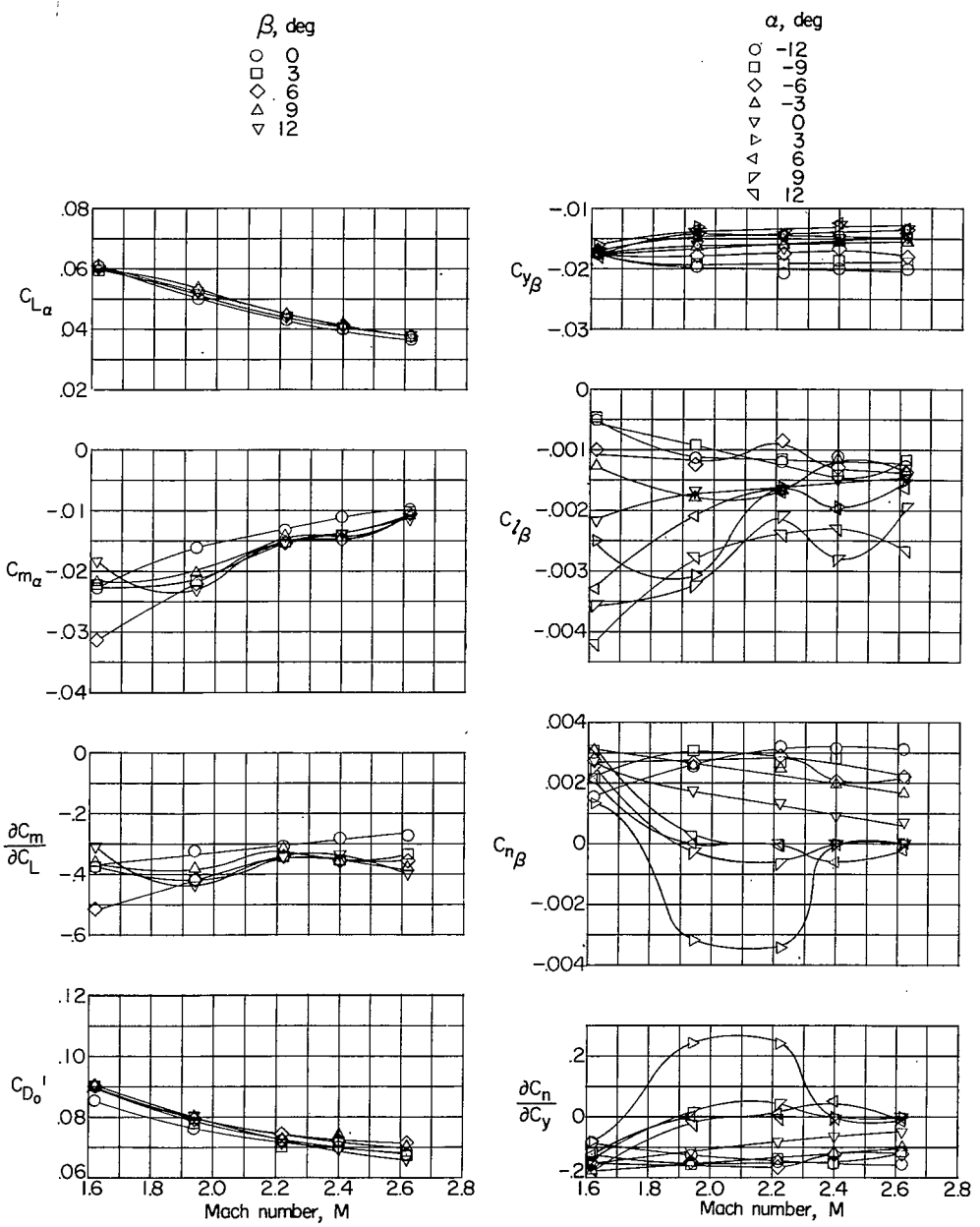

(a) Longitudinal stability derivatives for various constant angles of sideslip through $\alpha = 0^\circ$.

(b) Lateral stability derivatives for various constant angles of attack through $\beta = 0^\circ$.

Figure 7.- Plot of static longitudinal and lateral stability derivatives and minimum drag coefficient of the X-1E airplane against Mach number at combined angles of attack and sideslip.

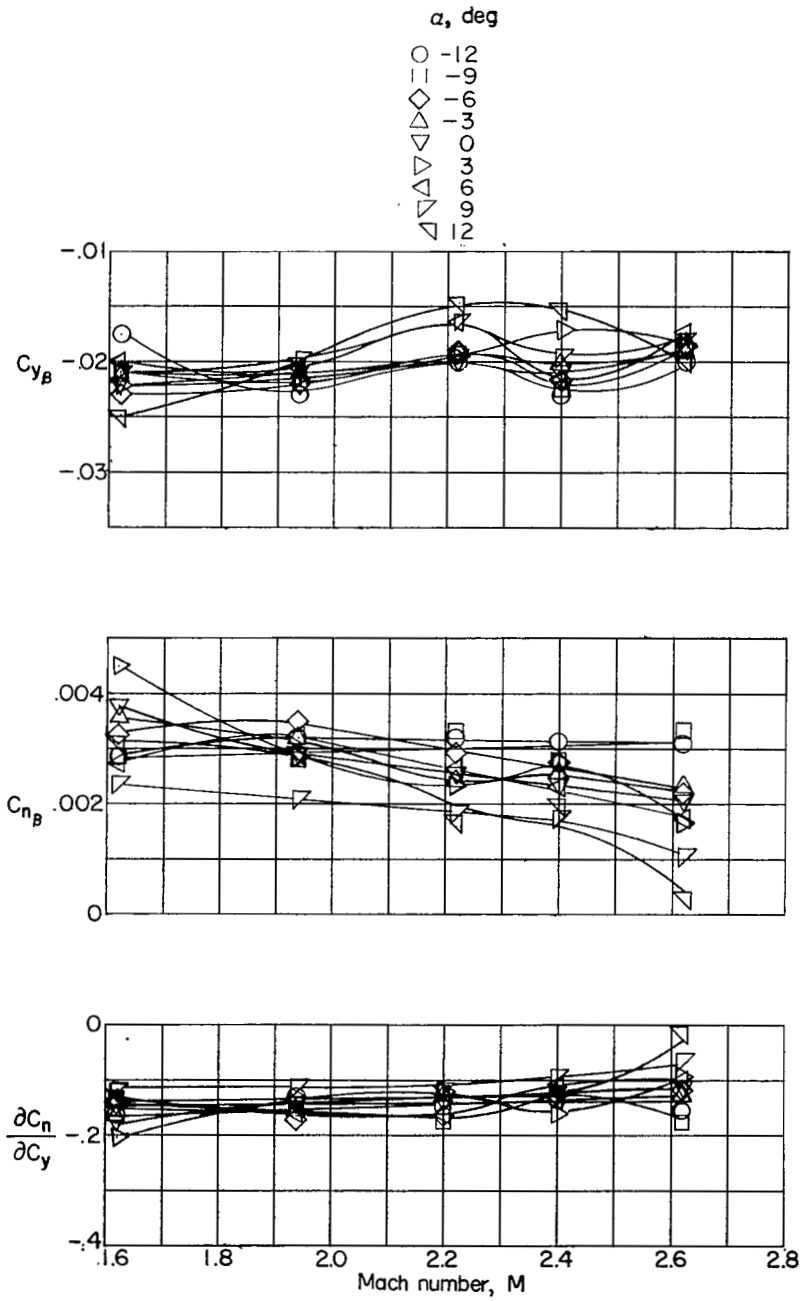

(c) Lateral stability derivatives for various constant angles of attack through $\beta = 8^\circ$.

Figure 7.- Concluded.

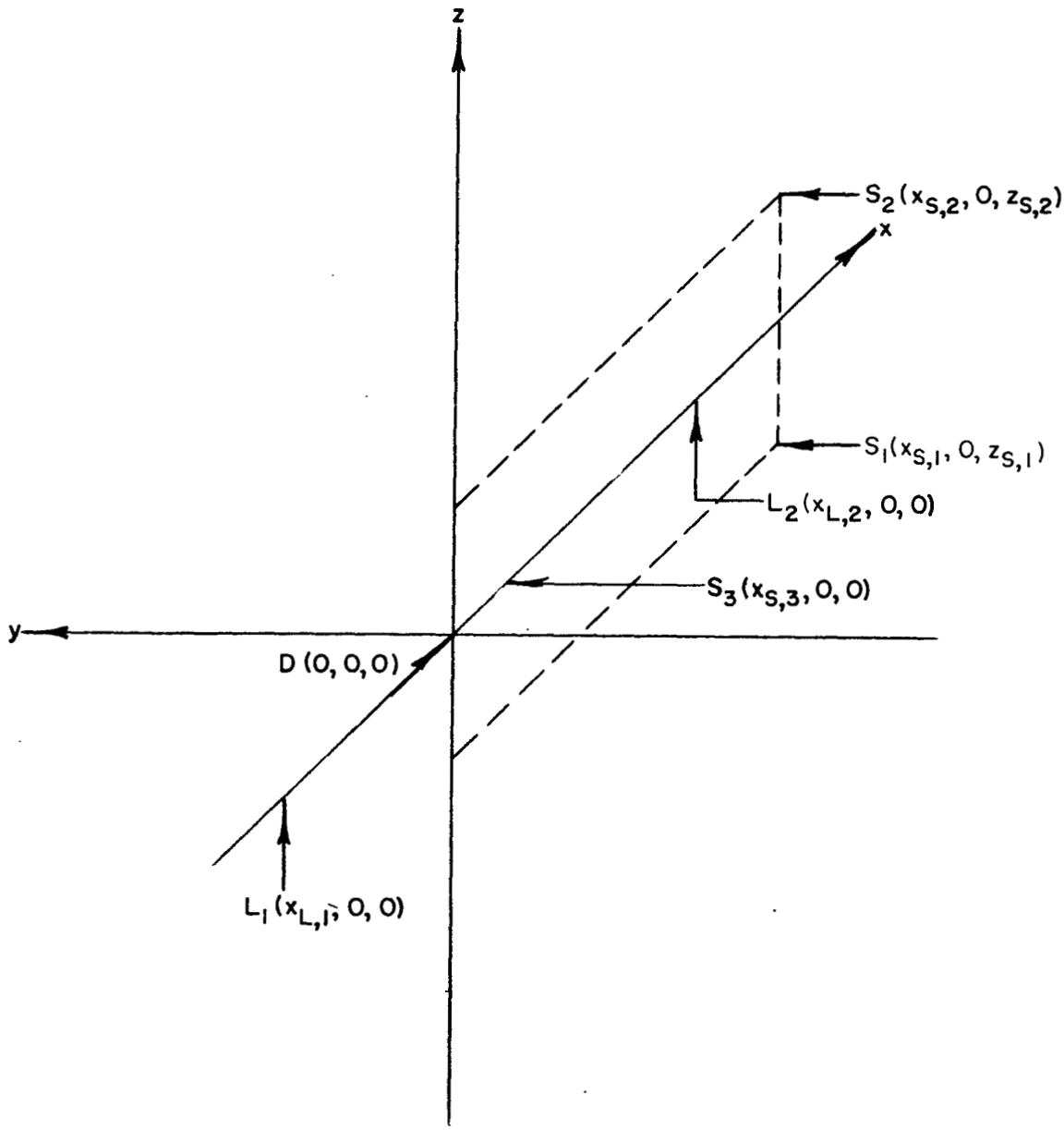

Figure 8.- Schematic of balance reaction force vectors in tunnel x-, y-, and z-axes.

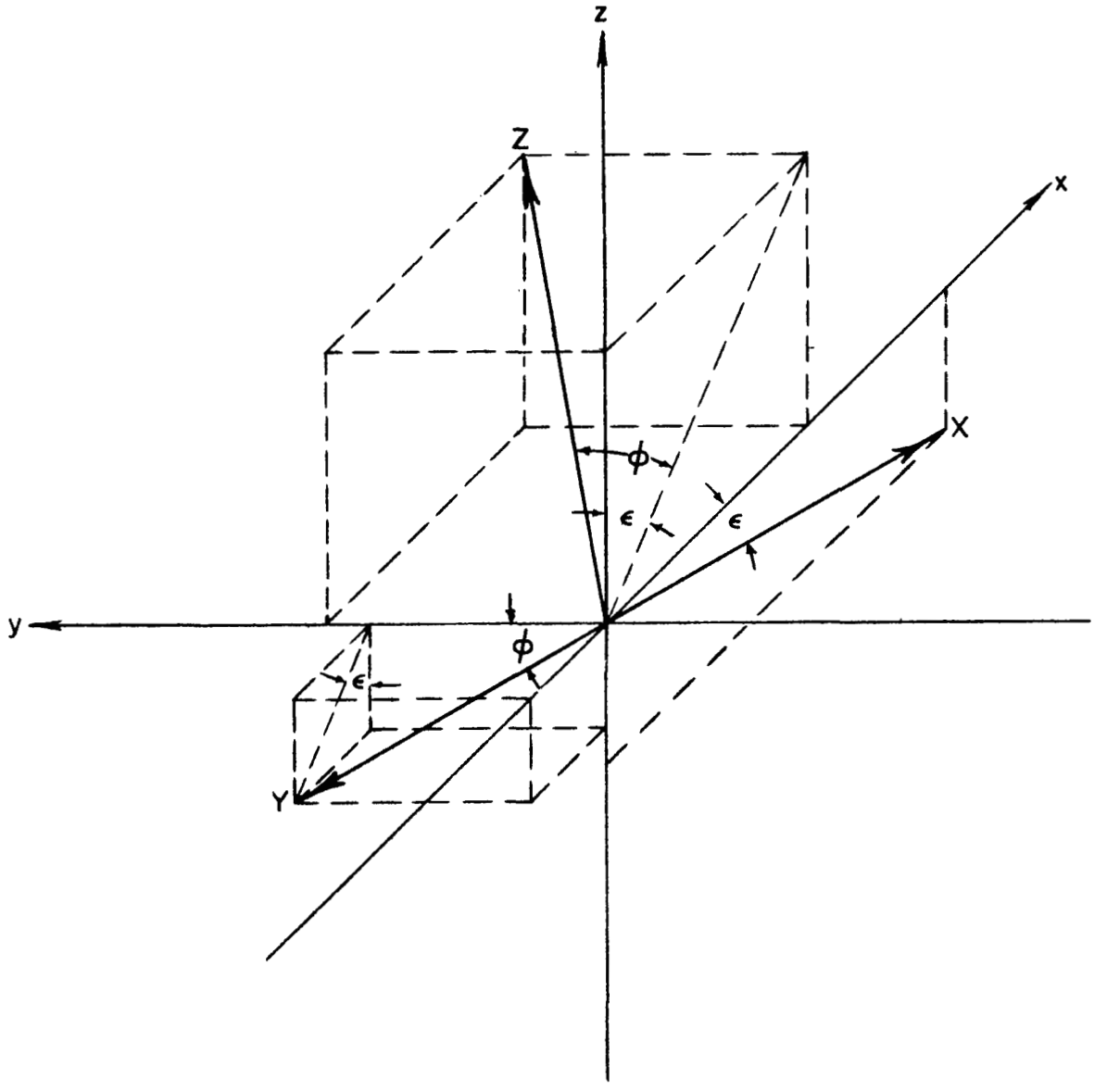

Figure 9.- Relationship of body X-, Y-, and Z-axes to tunnel x-, y-, and z-axes.

[redacted]

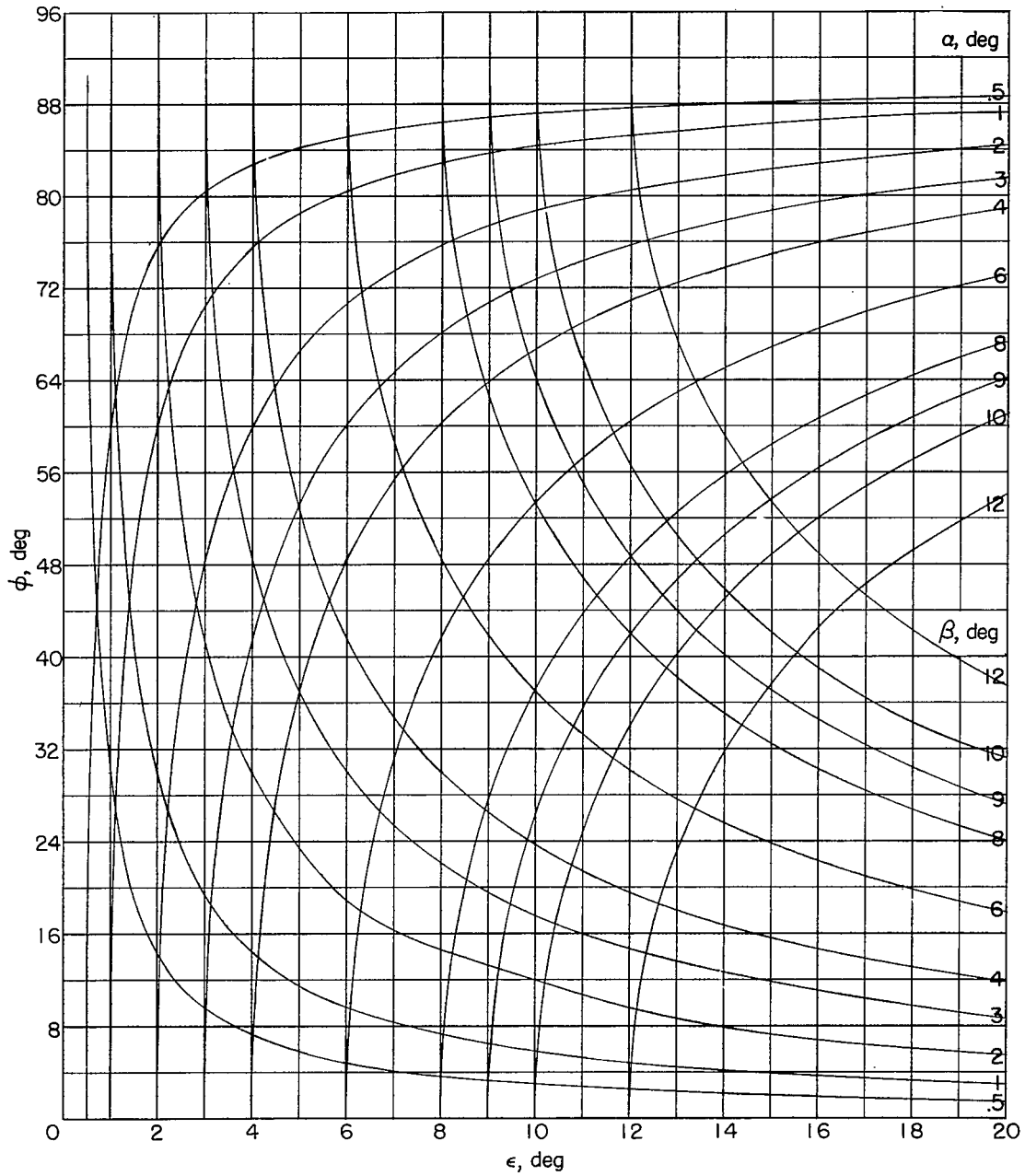

Figure 10.- Chart for determining φ and ϵ settings necessary to obtain desired combinations of α and β.